ck for updates

ChemPubSoc Europe

DOI: 10.1002/batt.201800148

BATTERIES & SUPERCAPS
Articles

Next-Generation Additive Manufacturing: Tailorable Graphene/Polylactic(acid) Filaments Allow the Fabrication of 3D Printable Porous Anodes for Utilisation within Lithium-Ion Batteries

Christopher W. Foster,[a] Guo-Qiang Zou,[b] Yunling Jiang,[b] Michael P. Down,[a] Christopher M. Liauw,[a] Alejandro Garcia-Miranda Ferrari,[a] Xiaobo Ji,[b] Graham C. Smith,[c] Peter J. Kelly,[a] and Craig E. Banks*[a]

Herein, we report the fabrication and application of Li-ion anodes for utilisation within Li-ion batteries, which are fabricated via additive manufacturing/3D printing (fused deposition modelling) using a bespoke graphene/polylactic acid (PLA) filament, where the graphene content can be readily tailored and controlled over the range 1–40 wt.%. We demonstrate that a graphene content of 20 wt.% exhibits sufficient conductivity and critically, effective 3D printability for the rapid manufacturing of 3D printed freestanding anodes (3DAs); simplifying the components of the Li-ion battery negating the need for a copper current collector. The 3DAs are physicochemically and electrochemically characterised and possess sufficient conductivity for electrochemical studies. Critically, it is found that if the 3DAs are used in Li-ion batteries the specific capacity is very poor but can be significantly improved through the use of a chemical pre-treatment. Such treatment induces an increased porosity, which results in a 200-fold increase (after anode stabilisation) of the specific capacity (ca. 500 mAh g^{-1} at a current density of 40 mA g^{-1}). This work significantly enhances the field of additive manufacturing/3D printed graphene based energy storage devices demonstrating that useful 3D printable batteries can be realised.

1. Introduction

With the environmental pressure to reduce fossil fuel usage and the ever-increasing demand upon energy consumption, there is currently a societal focus upon the fabrication of innovative energy production/storage devices.[1,2,3] Consequently, there has been a surge within the literature for research into the utilisation and understanding of novel nanomaterials such as graphene, carbon nanotubes and nanoalloys, which are providing a solid platform for the continued improvement within the efficiency and effectiveness of these novel energy storage devices, particularly within Li-based batteries.[4,5,6,7]

The understanding and application of these nanomaterials has generally focused upon the utilisation of two-dimensional printing methods, such as blade coatings, nonetheless research has now shifted to the incorporation of additive manufacturing (AM)/3D printing. AM/3D printing has attracted a large interest within the field of electrochemical energy storage due its ability to create large surface area structures, which can offer beneficial energy capabilities. The most utilised AM/3D printing techniques within the field of energy storage are typically based upon direct-writing technology, in which an active material dispersion is passed through a nozzle to create an intricate 3D structure.[8] Generally, the performance of these devices can outperform that of their 2D counterparts. For example, Sun *et al.*[9] have utilised this direct-ink writing protocol to 3D print lithium-based nanocomposites $Li_4Ti_5O_{12}$ (LTO) and $LiFePO_4$ (LFP), exhibiting corresponding specific capacity values of 131 and 160 mAh g^{-1} respectively. However, it should be noted that the creation of devices using the direct-ink writing methodology are useful, but in many cases the incorporation of a complex post-production *ex-situ* step is required to solidify the device. For example García-Tuñon *et al.*[10] incorporate the use of freezing with liquid nitrogen following extrusion/printing, prior to application. Such approaches are extremely limited to simple geometries with a height of less than 1 mm, with *in-situ* curing being paramount to the structural integrity of the AM/3D printed objects. To exploit the full potential of AM/3D printing (*i.e.* large/complex geometries) one must consider alternatives to these AM/3D printing technologies. Fused deposition modelling (FDM) is one

[a] *Dr. C. W. Foster, Dr. M. P. Down, Dr. C. M. Liauw, Mr. A. Garcia-Miranda Ferrari, Prof. P. J. Kelly, Prof. C. E. Banks*
Faculty of Science and Engineering, Manchester Metropolitan University, Chester Street, Manchester M15 GD, UK
Tel: ++(0)1612471196
Fax: ++(0)1612476831
E-mail: c.banks@mmu.ac.uk
Homepage: www.craigbanksresearch.com
[b] *Dr. G.-Q. Zou, Y. Jiang, Prof. X. Ji*
College of Chemistry and Chemical Engineering, Central South University, Changsha 410083, China
[c] *Prof. G. C. Smith*
Faculty of Science and Engineering, Department of Natural Sciences, University of Chester, Thornton Science Park, Pool Lane, Ince, Chester CH2 4NU, UK

Supporting information for this article is available on the WWW under https://doi.org/10.1002/batt.201800148

© 2019 Wiley-VCH Verlag GmbH & Co. KGaA, Weinheim

of the most popular additive manufacturing techniques as it allows a 3D printed object to be cured *in-situ,* without recourse to complex and time-consuming post-processing. One considerable challenge for FDM printing is the realisation of thermoplastic filaments with high filler (*active material*) content, which can be successfully printed. Generally, the currently commercially available 3D filaments contain low amounts of active materials within the 3D printable filaments, offering little applicability and ability to be useful in the field of electrochemistry. For example, Wei et al. have recently fabricated and partially characterised graphitic-based polylactic acid (PLA) and acrylonitrile-butadiene-styrene (ABS) conductive filaments (with graphene loadings of up to 5.6 *wt.*%); in this case there is a very low amount of graphene that is incorporated into the filament as higher amounts results in a filament, which is unable to be 3D printed due to aggregation of the graphene blocking the nozzle. Recently, we have examined a novel graphene/poly(lactic) acid filament (PLA), that could be successfully AM/3D printed into useful electrochemical geometries.[11] However, this filament only possessed ~8 *wt.*% active (graphene) material. Nonetheless, this study offered a potentially insightful and innovative bottom-up fabrication method route for the production of energy storage devices.

In this paper, we report the application of AM/3D printed Li-ion anodes, fabricated *via* a facile fused deposition modelling technique using bespoke 3D printable graphene/PLA filaments, where the graphene content can be readily tailored and controlled over the range 1–40 *wt.*%. Physicochemical and electrochemical characterisation is performed allowing for optimisation of the graphene content to allow control over the 3D printability, conductivity and electrochemical activity of 3D printed freestanding anodes (3DAs); this approach simplifies the components of the Li-ion battery negating the need for a copper current collector.

2. Results and Discussion

2.1. Development and Optimisation of the Bespoke Graphene/PLA Filaments

AM/3D printable graphene/poly(lactic) acid (PLA) filaments were created with a range of graphene-loaded PLA filaments containing 1, 5, 15, 20 and 40 *wt.*%. graphene nanoplatelets, *validated* by thermogravimetric analysis (TGA, see Figure 1A); the detailed fabrication is reported within the Methods Section, with subsequent electrochemical characterisation and rationalisation (cyclic voltammetry, heterogeneous electron transfer rate analysis) in the ESI. In brief, the fabrication of graphene/PLA filaments containing percentages over 20 *wt.*% are extremely brittle and highly unreproducible in terms of both homogeneity, printability and structural integrity; additionally filaments with a *wt.*% of graphene below 10% did not offer sufficient percolation (*i.e.* high resistivity), as can be seen within Figure 1B and did not create an electrochemically useful platform. Therefore, we have found that 15–20% is the optimal *wt.*% when one is considering graphene nanoplatelets, as described in Figure 1B, where the resistivity decreases and conductivity increases. Upon consideration of the topography (TEM and SEM; Figure 1C and Figure S1B respectively) of the graphene powder at 20 *wt.*% (used to create the graphene/PLA filament), it is clearly illustrated, that the graphene is dispersed creating a conductive network throughout the graphene/PLA

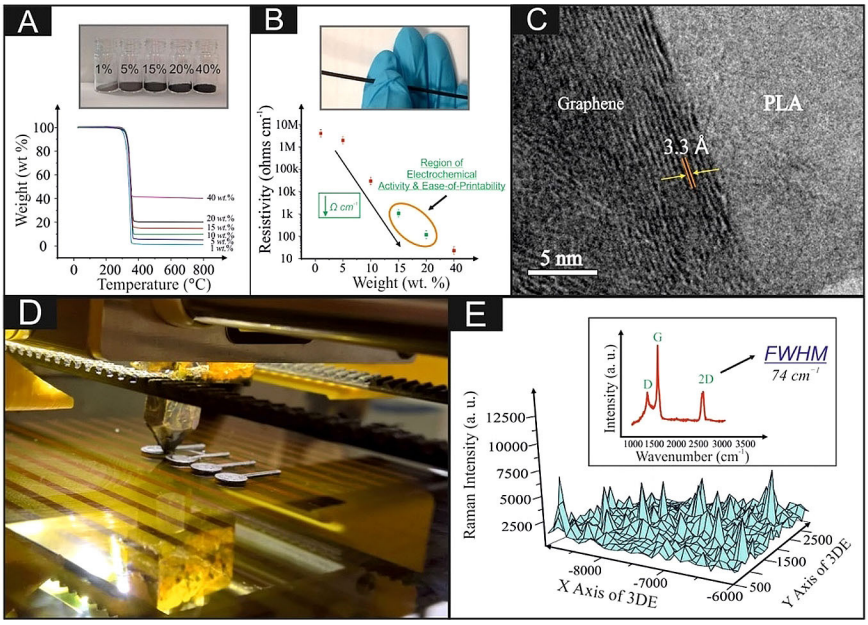

Figure 1. Physicochemical characterisation and optical images of the graphene/PLA powders, respective filaments and 3DAs. A: Thermogravimetric analysis, B: Resistivity *vs.* graphene content, C: TEM analysis of 20 *wt.*% graphene/PLA, D: 3D printing process of the 3DAs (for electrochemical characterisation), E: Raman (inset) and Raman Mapping of the 3DA. *Note: the Raman mapping is of the 2D band at ca. 2600 cm^{1-} (Full width half maximum (FWHM): 74 cm^{-1}).*

© 2019 Wiley-VCH Verlag GmbH & Co. KGaA, Weinheim

25666223, 2019, 5, Downloaded from https://chemistry-europe.onlinelibrary.wiley.com/doi/10.1002/batt.201800148 by University of Ulsan, Wiley Online Library on [11/11/2025]. See the Terms and Conditions (https://onlinelibrary.wiley.com/terms-and-conditions) on Wiley Online Library for rules of use; OA articles are governed by the applicable Creative Commons License

filament, corroborating with the aforementioned increased conductivity and electrochemical activity (Figure S1C).

After optimisation of the graphene content, the graphene/PLA filament containing 20 *wt.*% graphene was 3D printed producing a test anode with a diameter of 3 mm and a thickness of 1 mm (described within the Methods Section and exhibited in Figure 1D) for further physicochemical characterisation. Raman analysis was performed on the 3D printed graphene anodes (3DA), (inset of Figure 1E) where characteristic graphitic D, G and 2D peaks are present at ~1300, 1600 and 2700 cm^{-1} respectively. The Raman spectra indicates that the AM/3D printing of the graphene/PLA results in agglomeration of the graphene sheets, which is as expected and has been postulated within previously reported literature.[2,12,] This is further confirmed with full width half maximum (FWHM) analysis of the 2D peak exhibiting a value of 74 cm^{-1}, which is significantly larger than that of the corresponding values of FWHM analysis for monolayer or *quasi*-layer graphene, 28 cm^{-1}[13] and 58 cm^{-1}[14] respectively, indicating that the 3DA consists of multi-layer graphene.

Next, XPS analysis was undertaken with high-resolution scans made over the C 1s and O 1s photoelectron peaks. These were found to be broad and of an unusual peak shape. Fitting to known chemical state reference data caused some difficulty until it was observed that sub-sets of the components present appeared to shift by different amounts under different conditions of charge neutralisation. This indicates that the samples contained materials of differing electrical conductivity and therefore exhibited this differential charging effect. The components presented in Figure S3 were identified as: *i*) the carbon phase (graphene), with some PLA bound to it exhibiting the same conductivity and an isolated PLA phase not bound to the carbon phase, thus acting essentially as an insulator. A sharp and intense peak in the range 284.5 eV–285.0 eV to represent C–C bonds and a weak broad peak in the range 290.5–292.0 eV[15] at between 5 and 8% of the first peak above, to represent graphitic plasmon losses. A group of three peaks separated by 1.6 eV and of the same line-shape and intensity to represent the C–C, C–O and C(=O)O components of PLA. When the charge neutralisation conditions of the measurement were varied, this group maintained a fixed relationship to the main C–C peak above and, therefore, represents PLA intimately bound to the graphene component. Nonetheless, the PLA was present in two forms. The conducting and insulating PLA phases were at approximately the same levels in the graphene/PLA samples, as judged from the relative intensities of their components in the C 1s peak. The O 1s peaks show the same differential charging phenomena as the C 1s peaks (Figure S3). The O 1s could be modelled using two sets of coupled components of equal intensity representing C–O and C=O in PLA, along with a low intensity further component representing oxygen bound directly to the graphene. The presence of such oxygen, although at low levels, would add to the complexity of the C 1s peak envelope and may account for the imperfect fits obtained with the model used. In summary, XPS analysis reveals that the high volume of graphene within the graphene/PLA filament is fully dispersed within the PLA creating a conductive pathway throughout the sample, thus corroborating with aforementioned electrochemical and physicochemical characterisation.

2.2. Energy Capabilities of the Additive Manufactured/3D Printed Graphene/PLA 3DAs

The energy capabilities of the 3DAs were next evaluated within a Li-ion battery setup. As a model to benchmark and understand their performance, the anodes were AM/3D printed with the same geometries as a CR2016 coin cell (*i.e.* a diameter of 17.75 mm with a thickness of 1 mm) using a conventional fused deposition modelling 3D printer (as described within the Methods section). As reported in our previous work, these freestanding anodes do not require a copper current collector. It is important to note, as exhibited within Figure 2, that these graphene 3DAs *as-is,* do not provide a highly beneficial electrochemical response. Providing an initial capacity of ~20 mAh g^{-1}, at a current density of 40 mA g^{-1}, with a substantial capacity loss over the remaining subsequent 200 scans. To understand such low electrochemical behaviour, we next analyse the topography of the graphene 3DA, Figure 2 presents SEM images where it is evident that the surface of the 3DA provides sufficient percolation, however do not offer an effective porosity for electrolyte wetting. In order to overcome this limitation, we next induce porosity within the 3DAs, by introducing a simple chemical pre-treatment using NaOH (see Methods section for more details). After this 24 hour pre-treatment the anode material offers a significantly improved porosity, which has been reflected in a contact angle study, where the unmodified 3DA exhibits an average angle ($N=6$) of 83.61° whereas the chemically treated 3DA provide an extremely low contact angle hysteresis. The porosity is also apparent upon SEM analysis of the chemically treated 3DA, presented within Figure 2 and Figure S4, where it is apparent that the thermoplastic upon the electrode surface has large voids, thus allowing more electrolyte to react with the 3DA. To ensure the full understanding of this modified 3DA, XPS was carried out upon a chemically treated sample (Figure S3) where it is apparent that the material has become more graphitic in nature. The crystalline structure of the graphene/PLA before and after chemical pre-treatment was analysed *via* X-ray diffraction (XRD). Depicted within Figure S5 are XRD patterns for the graphene/PLA and chemically pre-treated graphene, it is clear that the expected multi-layer graphene (002) peak appears in both cases, however the inclusion of a multi-layer graphene oxide (001) peak is apparent within the graphene/PLA, which is removed upon chemical pre-treatment.[16,17] It is important to understand that this material did not lose its 3D structure, as shown with TGA analysis in Figure S6, where the percentage of graphene remains at 20 *wt.*%, and integrity, but now offers an excellent electrochemical behaviour/performance. This AM/3D printed thermoplastic, exhibits an initial charge of ~1100 mAh g^{-1} (at a current density of 40 mA g^{-1}) after formation of the solid electrode interface (SEI) between scans 2–20, a capacity of 590 to 300 mAh g^{-1} was realised,

© 2019 Wiley-VCH Verlag GmbH & Co. KGaA, Weinheim

25666223, 2019, 5, Downloaded from https://chemistry-europe.onlinelibrary.wiley.com/doi/10.1002/batt.201800148 by University of Ulsan, Wiley Online Library on [11/11/2025]. See the Terms and Conditions (https://onlinelibrary.wiley.com/terms-and-conditions) on Wiley Online Library for rules of use; OA articles are governed by the applicable Creative Commons License

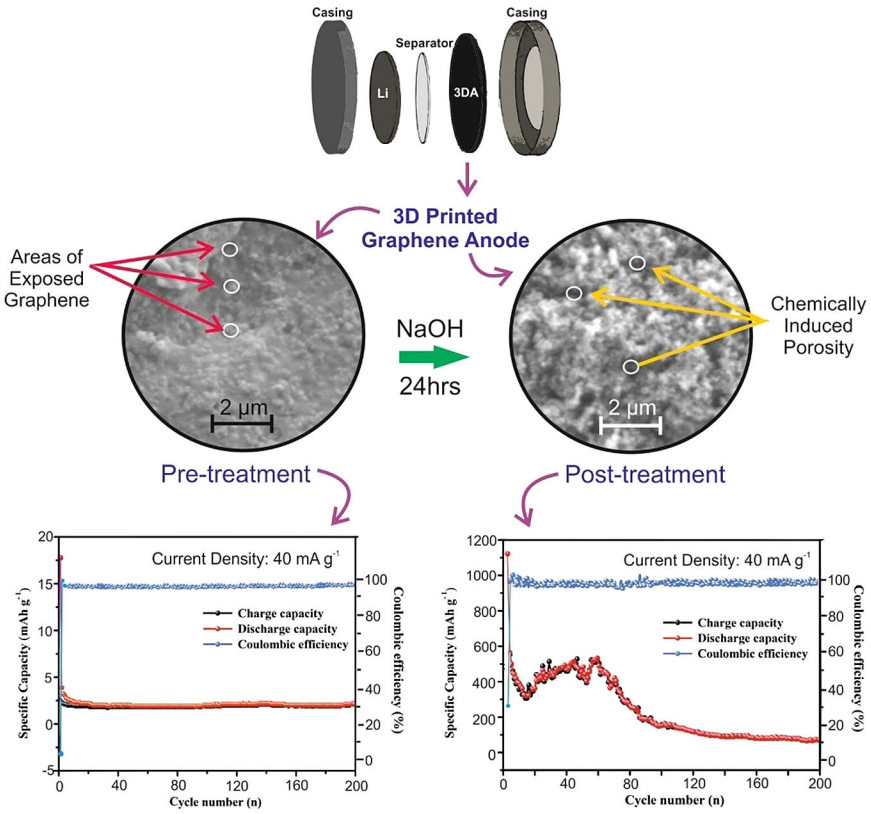

Figure 2. SEM images of a typical graphene 3DA *pre-* and *post*-NaOH chemical treatment displaying their respective charge-discharge profiles. *Note: the setup used to test the anodes is simpler over traditional coin cells as no copper current collector is required.*

increasing back to 500 mAh g^{-1} between scans 60–80, due to the electrochemical activation of the anode surface, allowing access to more electrolyte. After 80 scans, a stabilisation of the anode was demonstrated, with a specific capacity ranging between ~200 and 100 mAh g^{-1} (Figure 2). To understand the electrochemical process further cyclic voltammetric (CV) analyses were carried out at 0.1 mVs^{-1} (presented in Figure S7) where it is clear that the CV exhibits typical behaviour of a graphitic anode material.[18,19] It is also clear that on the first scan at ~0.5 V, the creation of the SEI layer is apparent, and upon subsequent scans, the material enters the stabilisation process. Also depicted in Figure S7 are charge-discharge profiles for a range of scan numbers (1st, 10th, 20th and 50th), where upon the 1st scan there is a reversible potential of ~0.75 V reducing to ~0.3 V upon repeated scanning. When comparing these specific capacities to that of the theoretical capacities for graphene and graphite (744 and 375 mAh g^{-1} respectively),[20] it is clear after the stabilisation of the anode that the specific capacities are larger than graphite but lower than graphene. Therefore, we suggest that the graphene incorporated within the 3DA, is predominantly graphene-like in its electrochemical behaviour, and that the increased surface area of the graphene nanoplatelets within the composite provide the improved energy outputs. The results presented herein enhances the field of additive manufacturing/3D printed graphene-based energy storage devices with the utilisation of a tailorable graphene/PLA filament, and with a simple chemical treatment of the 3D printed anode can exhibit a 200-*fold* increase within the specific capacity (after anode stabilisation).

3. Conclusions

For the first time, we report the fabrication and application of Li-ion anodes for utilisation within Li-ion batteries, using a bespoke graphene/PLA filament, in which the graphene content can be readily tailored and controlled (1–40 *wt.*%). It is found that with a graphene content of 20 *wt.*% the 3D printed freestanding anodes (3DAs) provide effective conductivity and 3D printability. Upon application of these anodes within a Li-ion battery, the initial specific capacity is very poor, however a simple chemical pre-treatment that can induce porosity results in a 200-fold increase (after anode stabilisation) of the specific capacity (ca. 500 mAh g^{-1} at a current density of 40 mA g^{-1}). The results presented herein significantly enhance the field of additive manufacturing/3D printed graphene based energy storage devices demonstrating that useful 3D printable batteries can be realised.

Methods

All chemicals used were obtained from Sigma-Aldrich at an analytical grade and were used without any further purification. All

© 2019 Wiley-VCH Verlag GmbH & Co. KGaA, Weinheim

25666223, 2019, 5, Downloaded from https://chemistry-europe.onlinelibrary.wiley.com/doi/10.1002/batt.201800148 by University of Ulsan, Wiley Online Library on [11/11/2025]. See the Terms and Conditions (https://onlinelibrary.wiley.com/terms-and-conditions) on Wiley Online Library for rules of use; OA articles are governed by the applicable Creative Commons License

25666223, 2019, 5, Downloaded from https://chemistry-europe.onlinelibrary.wiley.com/doi/10.1002/batt.201800148 by University of Ulsan, Wiley Online Library on [11/11/2025]. See the Terms and Conditions (https://onlinelibrary.wiley.com/terms-and-conditions) on Wiley Online Library for rules of use; OA articles are governed by the applicable Creative Commons License

solutions were prepared with deionised water of resistivity not less than 18.2 MΩ cm. Voltammetric measurements were carried out using an Autolab PGSTAT100 (Metrohm, The Netherlands) potentiostat.

Graphene/PLA filaments were fabricated by pre-mixing graphene and PLA utilising a facile solution based mixing step, briefly the graphene was dispersed within xylene and heated (under reflux) at 160 °C for 3 hours, the PLA was then added to the mixture and left for a further 3 hours. The resulting homogenous (solution phase) mixture then was then recrystallized within methanol, and left to dry (at 50 °C within a fan oven) until the xylene had evaporated. The resulting graphene-loaded PLA *powder* mix was then placed within a MiniCTW twin-screw extruder (ThermoScientific) at a temperature of 200 °C and a screw speed of 30 rpm, the diameter (1.75 mm) of the filament was controlled with a specific die with a set diameter. The 3D printed designs were fabricated using a ZMorph® printer (Warsaw, Poland) with a direct drive extruder at a temperature of 190 °C. The 3D printed designs were drawn *via* Fusion 360 (Autodesk, UK), to create a circular disc electrode with a range of diameters with a thickness of 1.0 mm. The potentiostatic electrochemical experiments were carried out utilising a three-electrode setup with either the graphene/PLA filaments or 3D printed anodes (3DA) as the working electrode (with a diameter of 3 mm and a thickness of 1 mm), and Ag/AgCl and platinum as the reference and counter electrodes, respectively. Each 3DA for these electrochemical characterisation experiments were printed with a connecting strip allowing simple connection to a crocodile clip. Chemical pretreatment of the 3DAs was carried out over range of 5–24 hours using 1 M NaOH, upon removed were soaked and washed with deionised water.

CR2016-type coin cells were assembled inside a mBraun glovebox ($H_2O < 0.5$ ppm, $O_2 < 0.5$ ppm) using the metallic lithium counter/reference electrode, a polypropylene separator (Celgard 2400), an electrolyte of 1 M $LiPF_6$ in ethylene carbonate and dimethyl carbonate (EC–DMC, 1:1) and a 3DA (with a diameter of 17.75 mm and a thickness of 1 mm). Charge-discharge measurements were carried out galvanostatically over a voltage range of 0.01–3.00 V using the Arbin battery test system (BT2000).

Scanning electron microscope (SEM) images and surface element analysis were obtained with a JEOL JSM-5600LV model equipped with an energy-dispersive X-ray (EDX) microanalysis package. Raman spectroscopy was performed using a Renishaw InVia spectrometer with a confocal microscope (×50 objective) spectrometer with an argon laser (514.3 nm excitation) at a very low laser power level (0.8 mW) to avoid any heating effects. Thermogravimetric analysis (TGA) was conducted utilising a PerkinElmer TGA 4000. The PLA samples were subject to a gradual temperature increase of 10 °C per minute, over a range between 25–800 °C, under a flow of nitrogen (40 ml/min). The X-ray photoelectron spectroscopy (XPS) data was acquired using a bespoke ultra-high vacuum system fitted with a Specs GmbH Focus 500 monochromated Al Kα X-ray source, Specs GmbH Phoibos 150 mm mean radius hemispherical analyser with 9-channeltron detection, and a Specs GmbH FG20 charge neutralising electron gun. Survey spectra were acquired over the binding energy range 1100–0 eV using a pass energy of 50 eV and high-resolution scans were made over the C 1s and O 1s lines using a pass energy of 20 eV. Under these conditions the full width at half maximum of the Ag $3d_{5/2}$ reference line is ~ 0.7 eV. In each case, the analysis was an area-average over a region approximately 1.4 mm in diameter on the sample surface, using the 7 mm diameter aperture and lens magnification of ×5. The energy scale of the instrument is calibrated according to ISO 15472, and the intensity scale is calibrated using an in-house method traceable to the UK National Physical Laboratory. Data was quantified using Scofield cross sections corrected for the energy dependencies of the electron attenuation lengths and the instrument transmission. Data interpretation was carried out using CasaXPS software v2.3.16. Contact angle measurements were carried out by evaluating an array of positions upon the 3DA.

The heterogeneous electron transfer rate constant, k^0_{obs}, were determined utilising the Nicholson method through the use of the following equation: $\psi = k^0_{obs}[\pi D n \nu F/(RT)]^{-1/2}$ where ψ is the kinetic parameter, D is the diffusion coefficient, n is the number of electrons involved in the process, F is the Faraday constant, R is the universal gas constant and T is the temperature.[21] The kinetic parameter, ψ, is tabulated as a function of ΔE_p (peak-to-peak separation) at a set temperature (298 K) for a one-step, one electron process with a transfer coefficient, α, equal to 0.5. The function of ψ (ΔE_p), which fits Nicholson's data, for practical usage (rather than producing a working curve) is given by: $\psi = (-0.6288 + 0.0021X)/(1 - 0.017X)$ where $X = \Delta E_p$ is used to determine ψ as a function of ΔE_p from the experimentally recorded voltammetry; from this, a plot of ψ against $[\pi D n \nu F/(RT)]^{-1/2}$ allows the k^0_{obs} to be readily determined.[22] The heterogeneous electron transfer rate constants were calculated assuming a diffusion coefficient of 9.10×10^{-6} cm^2 s^{-1} for hexaammineruthenium (III) chloride.[23].

Contributions

C.E.B conceived the concept. C.W.F, C.E.B, P.J.K and X.J. designed the experiments. C.W.F, C.M.L, M.P.D, A.G-M.F undertook the polymer related experiments. C.W.F, G-Q.Z, Y.J, X.J and C.E.B performed data analysis. G.C.S performed the XPS and its analysis. C.W.F and C.E.B wrote the manuscript, and all the authors discussed the results, contributed to the draft of the manuscript and commented on the final version. C.E.B coordinated the overall project.

Acknowledgments

Funding from the Engineering and Physical Sciences Research Council (Reference: EP/N001877/1) is acknowledged.

Conflict of Interest

The authors declare no conflict of interest.

Keywords: additive manufacturing · energy storage · graphene · lithium-ion batteries · 3D printing

[1] X. Zhang, L. Hou, A. Ciesielski, P. Samorì, *Adv. Energy Mater.* **2016**, *6*, 1600671-n/a.
[2] S. J. Rowley-Neale, C. W. Foster, G. C. Smith, D. A. C. Brownson, C. E. Banks, *Sustainable Energy & Fuels* **2017**, *1*, 74–83; Fuels **2017**, 1, 74–83.
[3] A. S. Aricò, P. Bruce, B. Scrosati, J.-M. Tarascon, W. van Schalkwijk, *Nat. Mater.* **2005**, *4*, 366.
[4] P. G. Bruce, B. Scrosati, J.-M. Tarascon, *Angew. Chem. Int. Ed.* **2008**, *47*, 2930–2946; *Angew. Chem.* **2008**, *120*, 2972–2989.
[5] D. Werner, D. H. Apaydin, E. Portenkirchner, *Batteries & Supercaps* **2018**, *1*, 160–168; Supercaps **2018**, 1, 160–168.

© 2019 Wiley-VCH Verlag GmbH & Co. KGaA, Weinheim

[6] M. Arnaiz, P. Huang, J. Ajuria, T. Rojo, E. Goikolea, A. Balducci, *Batteries & Supercaps* **2018**, *1*, 204–208; Supercaps **2018**, 1, 204–208.
[7] Q. Sun, K. C. Lau, D. Geng, X. Meng, *Batteries & Supercaps* **2018**, *1*, 41–68; Supercaps **2018**, 1, 41–68.
[8] A. Ambrosi, M. Pumera, *Chem. Soc. Rev.* **2016**, *45*, 2740–2755.
[9] K. Sun, T.-S. Wei, B. Y. Ahn, J. Y. Seo, S. J. Dillon, J. A. Lewis, *Adv. Mater.* **2013**, *25*, 4539–4543.
[10] E. García-Tuñon, S. Barg, J. Franco, R. Bell, S. Eslava, E. D'Elia, R. C. Maher, F. Guitian, E. Saiz, *Adv. Mater.* **2015**, *27*, 1688–1693.
[11] C. W. Foster, M. P. Down, Y. Zhang, X. Ji, S. J. Rowley-Neale, G. C. Smith, P. J. Kelly, C. E. Banks, *Sci. Rep.* **2017**, *7*, 42233.
[12] X. Wei, D. Li, W. Jiang, Z. Gu, X. Wang, Z. Zhang, Z. Sun, *Sci. Rep.* **2015**, *5*, 11181.
[13] K. Kim, S. Coh, L. Z. Tan, W. Regan, J. M. Yuk, E. Chatterjee, M. F. Crommie, M. L. Cohen, S. G. Louie, A. Zettl, *Phys. Rev. Lett.* **2012**, *108*, 246103.
[14] Z. Lin, X. Ye, J. Han, Q. Chen, P. Fan, H. Zhang, D. Xie, H. Zhu, M. Zhong, *Sci. Rep.* **2015**, *5*, 11662.
[15] G. Gao, D. Liu, S. Tang, C. Huang, M. He, Y. Guo, X. Sun, B. Gao, *Sci. Rep.* **2016**, *6*, 20034.
[16] T. Kar, R. Devivaraprasad, R. K. Singh, B. Bera, M. Neergat, *RSC Adv.* **2014**, *4*, 57781–57790.
[17] F. Abbate dos Santos, M. I. Bruno Tavares, *Polym. Test.* **2015**, *47*, 92–100.
[18] Zhihua Guo, Chengyang Wang, Mingming Chen, M. Li, *Int. J. Electrochem. Sci.* **2013**, *8*, 249.
[19] B. K. Antonopoulos, F. Maglia, F. Schmidt-Stein, J. P. Schmidt, H. E. Hoster, *Batteries & Supercaps* **2018**, *1*, 110–121; Supercaps **2018**, 1, 110–121.
[20] G. Wang, X. Shen, J. Yao, J. Park, *Carbon* **2009**, *47*, 2049–2053.
[21] R. S. Nicholson, *Anal. Chem.* **1965**, *37*, 1351–1355.
[22] I. Lavagnini, R. Antiochia, F. Magno, *Electroanalysis* **2004**, *16*, 505–506.
[23] C. E. Banks, R. G. Compton, A. C. Fisher, I. E. Henley, *Phys. Chem. Chem. Phys.* **2004**, *6*, 3147–3152.

Manuscript received: December 23, 2018
Revised manuscript received: February 7, 2019
Version of record online: April 2, 2019

© 2019 Wiley-VCH Verlag GmbH & Co. KGaA, Weinheim

25666223, 2019, 5, Downloaded from https://chemistry-europe.onlinelibrary.wiley.com/doi/10.1002/batt.201800148 by University of Ulsan, Wiley Online Library on [11/11/2025]. See the Terms and Conditions (https://onlinelibrary.wiley.com/terms-and-conditions) on Wiley Online Library for rules of use; OA articles are governed by the applicable Creative Commons License